Renewable Energy 71 (2014) 509–517

Contents lists available at ScienceDirect

Renewable Energy

journal homepage: www.elsevier.com/locate/renene

Tidal energy site resource assessment in the East River tidal strait, near Roosevelt Island, New York, New York

Budi Gunawan [a, *], Vincent S. Neary [a], Jonathan Colby [b]

[a] Water Power Technologies, Sandia National Laboratories, PO 5800, 1515 Eubank Ave., Albuquerque, NM 87185-1124, USA
[b] Verdant Power, Inc., The Octagon, 888 Main Street, Suite 1, New York, NY 10044-0213, USA

ARTICLE INFO

Article history:
Received 14 February 2013
Accepted 1 June 2014
Available online 22 June 2014

Keywords:
Acoustic Doppler velocimeter
Hub-height velocity measurements
Hydrokinetic power density
Roosevelt Island tidal energy site
Tidal energy converter
Turbulence

ABSTRACT

This study demonstrates a site resource assessment to examine the temporal variation of the current speeds, current directions, turbulence intensities, and power densities for a tidal energy site in the East River tidal strait. These variables were derived from two months of acoustic Doppler velocimeter (ADV) measurements at the design hub height of the Verdant Power Gen5 hydrokinetic turbine. The study site is a tidal strait that exhibits semi-diurnal tidal current characteristics, with a mean horizontal current speed of 1.4 m s^{-1}, and a turbulence intensity of 15% at a reference mean current of 2 m s^{-1}. Flood and ebb flow directions are nearly bi-directional, with a higher current speed during flood tide, which skews the power production towards the flood tide period. The tidal hydrodynamics at the site are highly regular, as indicated by the tidal current time series that resembles a sinusoidal function. This study also shows that the theoretical force and the power densities derived from the current measurements can be significantly influenced by the length of the time window used for averaging the current speed data. Furthermore, the theoretical power density at the site, derived from the current speed measurements, is one order of magnitude greater than that reported in the U.S. national resource assessment. This discrepancy highlights the importance of conducting site resource assessments based on measurements at the tidal energy converter device scale.

1. Introduction

The siting and design of a single tidal energy converter (TEC), or an array of TECs, requires characterization of the spatial and temporal variation of the current speed and the turbulence acting on the proposed energy extraction plane (EEP) of the TEC. This characterization is necessary in order to: 1) determine the hydrodynamic forces, array configuration, and resulting available power estimates over a representative period of record; and 2) design the structural loading and power capacity of the TEC. These characteristics influence project financing decisions that will support the development of pilot and commercial tidal projects.

Due to the deterministic nature of tidal hydrodynamics, which are predominantly governed by lunar and solar orbital cycles, it is generally accepted that temporal characteristics of tidal flows, including daily, spring, and neap tidal cycles, can be predicted with reasonable accuracy over the project life of a hydrokinetic turbine array. However, the hydrodynamic conditions can vary greatly over short distances [1]. In addition, current speed fluctuations due to turbulence at high frequencies (~10 Hz) can contribute significantly to the hydrokinetic energy resource [2]. National assessments of tidal current energy resources (e.g., [3–5]), while valuable for estimating the overall theoretical resource over a large area to advise national planning of tidal energy sites, do not provide the degree of spatial and temporal resolution required to site and design individual TECs or arrays. National assessments may also miss small "hot spots" that could be viable sites for TECs. High fidelity measurements, such as those collected in this study, can help address some of the known limitations of national scale assessments.

Best practices for tidal energy site resource assessments are in development [6], including the instruments needed for collecting current speed and turbulence measurements, deployment strategies for these instruments, and methods for post-processing and analyzing raw instrument measurements; however, such practices have yet to be universally adopted. Tidal energy site resource assessment studies, e.g. Refs. [7–12], are providing invaluable data

* Corresponding author. Tel.: +1 505 845 8869; fax: +1 505 844 6541.
E-mail addresses: budi.gunawan@sandia.gov, budi.gunawan@yahoo.com (B. Gunawan).

http://dx.doi.org/10.1016/j.renene.2014.06.002
0960-1481/

and experience that will help formulate and improve tidal energy site resource assessment practices, while also improving our knowledge of the range of hydrodynamic conditions that are present at tidal energy sites under consideration for commercial-scale projects.

Although an acoustic Doppler current profiler (ADCP) is commonly used for tidal energy site resource assessments (e.g., [1,6,9,13]), an ADCP does not typically have sufficient spatial and temporal resolution to characterize turbulence within the inertial and viscous sub-ranges. This shortcoming is due to its relatively low data output rate and large sampling volume. As such, an acoustic Doppler velocimeter (ADV), which typically has a higher data output rate and a smaller sampling volume than the ADCP, is often preferred for turbulence measurements. ADV measurements of all three components of the instantaneous velocity at the planned hub height centerline of the EEP are especially valuable for site hydrodynamic and resource characterization. ADV measurements can also be used to modify turbulent inflow models, e.g., TurbSim [14], to evaluate the effects of unsteady turbulent loading on TECs by providing accurate inflow boundary conditions for high fidelity computational fluid dynamics (CFD) and turbine design models such as FAST [15] and CACTUS [16].

Since long-term ADV measurements (>1 month duration) at many locations are expensive, and therefore impractical, moving-vessel ADCP measurements are still needed to determine the magnitude and spatial distribution of mean tidal current speeds and power densities at tidal energy sites. Developing cost-effective ADV deployment strategies and improving the accuracy of ADCP-derived turbulence measurements is an active area of research [7,12,17–23].

The goal of this study is to conduct a resource assessment based on ADV measurements collected at the centerline of the EEP of a TEC to be located at a tidal energy site. This study examines the temporal variability, frequency, duration, direction, and magnitude of variables such as mean current speed, turbulence, hydrodynamic force, tidal power and tidal energy over a two-month period. These parameters are derived from three instantaneous velocity components (u, v and w) measured at the proposed rotor hub height ($z_{hub} = 4.25$ m) of a Verdant Power Gen5 hydrokinetic turbine. In addition, the average power density, determined by measurements, is compared to the modeled value reported in the national tidal current energy resource assessment [3].

2. Study site

Verdant Power's Roosevelt Island Tidal Energy (RITE) site was licensed in January 2012 by the Federal Energy Regulatory Commission (FERC) for a 1.05 MW array of up to 30 turbines. FERC project No. 12611 is the first commercial pilot license for a tidal power project granted in the United States [24–27]. Infrastructure installed for previous turbine and instrument deployments at the site, and the federal and state permits obtained for such deployments, were important factors that helped facilitate the present study.

The RITE Project site boundary encompasses an area approximately 1000 m by 100 m in a distributary channel of the East River tidal strait, which connects Long Island Sound in the North and New York Harbor in the South. The site is located on the east side of Roosevelt Island, between the boroughs of Manhattan and Queens, New York City (Fig. 1a). The tidal currents are mainly driven by pressure head differences between the New York Harbor inlet to the South and the Long Island Sound outlet to the North [28]. The maximum flow rates at the site have yet to be quantified with certainty. Numerical models predict 7662 $m^3\ s^{-1}$ in one study [25], and 3571 $m^3\ s^{-1}$ in another [29]. The channel's Reynolds number (Re) at both of these maximum discharges and mean higher high water (MHHW) is on the order of 10^7. The Reynolds number was calculated using the channel's bulk current speed and water depth. The water depth is an approximate value of the channel's hydraulic radius, assuming a wide channel with a wetted perimeter nearly equal to the top width. NOAA tidal stations located at Horns Hook and Queensboro Bridge (Fig. 1a), and USGS Site No: 404810735538063 (Harlem River at Randall's Island), provide historical records of water surface levels (h) in close proximity to the study site [30]. The difference between the mean low water (MLW) and the mean high water (MHW), the mean tidal range, is 1.3 m.

3. Methods

The present study deployed two upward-looking Sontek 10 MHz ADVs at the RITE site. The ADVs were mounted on a tower and placed at a proposed deployment location for a Verdant axial-flow passive-yaw hydrokinetic turbine rotor (rotor radius $r = 2.5$ m). The locations of the ADVs are shown in Fig. 1b, with the positive x direction pointing along the ebb current. The x, y and z

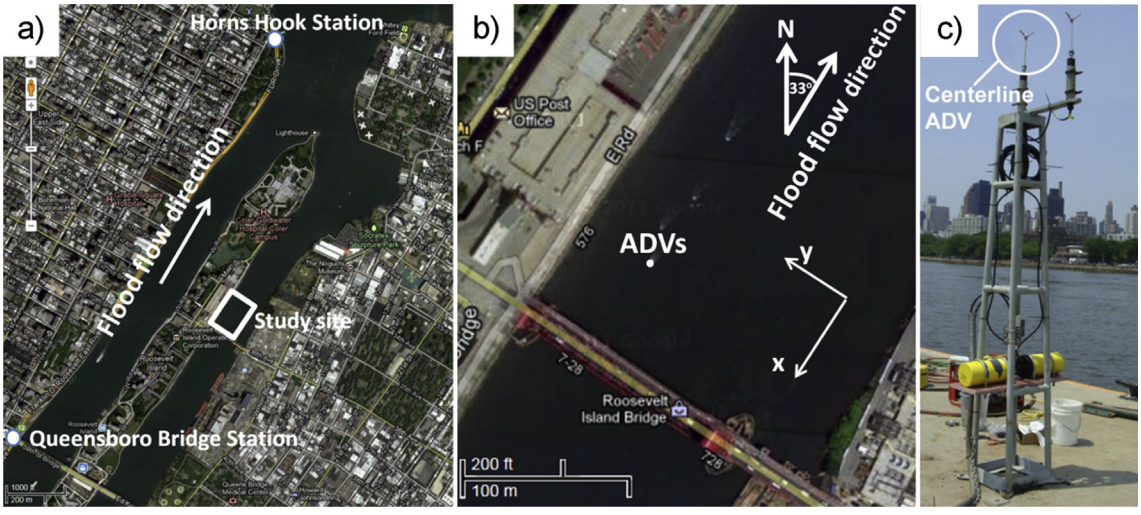

Fig. 1. (a) RITE study site and NOAA tidal stations (Horns Hook and Queensboro Bridge) in New York's East River Tidal Strait, (b) ADV tower location at the study site, and (c) ADV tower showing the two velocimeters.

axes of the ADV were closely aligned with the longitudinal, lateral, and vertical directions in the channel. The vertical component of the instantaneous velocity (w) was found to be negligible compared to the horizontal components, u and v. The ADVs measured the three instantaneous velocity components at the design turbine hub height ($z_{hub} = 4.25$ m); one located at the center point of the proposed rotor-plane and the other located 0.5 m from the center point in the same plane (Fig. 1c). The ADV sampling volumes were placed approximately 0.5 m above the top of the tower, to minimize the effects of the tower supports altering the current flow. In this study, only measurements from the centerline ADV are presented because the difference in the magnitude of the current speed and the spectral energy density derived from each velocimeter was not significant due to the short separation distance between the two ADVs. An attempt to synchronize the two ADVs was not successful.

In order to resolve most of the major tidal harmonic constituents, measurements over a minimum period of 35 days are required. This study collected data for 67 days, from 9 June to 15 August 2011. According to the criteria suggested by Nezu and Nakagawa [31] and García et al. [32], with the flow and geometric characteristics of the RITE site, a minimum of an 8 Hz ADV data output rate is required to adequately characterize turbulence down to the inertial sub-range. Data output rates of 20 Hz (between 9 June and 17 July) and 10 Hz (between 17 July and 15 August) were used. The velocity-range parameter for each ADV was set to 3.6 m s^{-1} to minimize signal aliasing in the horizontal current velocity measurements. Spikes, which can have a significant contribution to the total turbulent kinetic energy, were detected using the phase-space-thresholding (PST) method [33] and replaced with the overall average value of the time series using the data post-processing code described in Ref. [34]. Instantaneous values of hydrodynamic force per unit area (force density, FD) and power per unit area (power density, PD) were calculated using Equations (1) and (2):

$$\mathrm{FD} = \frac{F}{A} = \frac{1}{2}\rho\, u_c^2 \tag{1}$$

$$\mathrm{PD} = \frac{P}{A} = \frac{1}{2}\rho\, u_c^3 \tag{2}$$

where ρ is the water density (1025 kg m^{-3}) and u_c is the instantaneous horizontal current (m s^{-1}).

Turbulence intensities were calculated from ADV measurements over a time interval long enough to minimize the variations caused by large-scale eddies, but short enough to ensure the current speed within this period is relatively stationary. A five-minute window averaging time (WAT) for calculating the turbulence intensity was selected because it is the duration over which the time-averaged mean horizontal current ($\overline{u_c}$) and the root-mean-square (RMS) current horizontal current speed ($\sigma_{u_c} = \sqrt{\overline{u_c' u_c'}}$) converged. Fig. 2a and b show how $\overline{u_c}$ and σ_{u_c} values change with the WAT for six different datasets collected on 13 July 2011. The mean velocities and RMS of velocities fluctuate for WATs less than 180 s (3 min), because large-scale eddy effects are not completely smoothed by the averaging process. The mean velocities and RMS of velocities are smoothers for WATs greater than 180 s. However, their values gradually increase or decrease with respect to the WAT because of tidal changes. More pronounced gradients are observed when current speed magnitudes are relatively small (<1 m s^{-1}) during the slack tide period. Overall, the variables $\overline{u_c}$ and σ_u are relatively constant for WAT values between 3 and 5 min.

4. Results and discussion

4.1. Site characteristics

The semi-diurnal variation of the water level (h) and the variation of the corresponding five-minute-averaged horizontal current, $\overline{u_c}$, over a 4-day period around the full moon (spring tide) are shown in Fig. 3. The $\overline{u_c}$ values during this period oscillate between 0.0 and 2.4 m s^{-1}. There are two peak ebb and two peak flood current speeds, and two high-water levels and two low-water levels occurring in each tidal cycle. The average mean current speed over the entire period of record (POR) is 1.4 m s^{-1}, which is a reasonable estimate of the mean annual current speed for the RITE site. The daily peak flood and peak ebb current speeds ($\overline{u_{c_{max}}}$) occur at the inflection points of the water surface level time series (Fig. 3). The dominant tidal harmonic constituent at the RITE site is an M2 harmonic ($T = 12.42$ h), according to [30,35]. This was also shown in the spectral energy density plot of the instantaneous horizontal current speed (u_c) in the low frequency range $f \in [10^{-5}\ 10^{-3}]$ Hz (not shown) and in the calculations of major tidal current constituents and their amplitudes using the T_Tide Harmonic Analysis Toolbox code [36]. The results of the T_Tide harmonic analysis are presented in Table 1. The variable normalized amplitude is the amplitude of the constituents, normalized by the amplitude of the M2 constituent. The values of the normalized amplitude variable indicate that the M2, N2, and S2 harmonic constituents are the three most dominant constituents at the site.

Due to its relatively straight and uniform channel geometry, the tidal hydrodynamics at the RITE site are highly regular. The tidal current speed pattern resembles a sinusoidal function, with nearly constant current speeds for every peak ebb and peak flood tide.

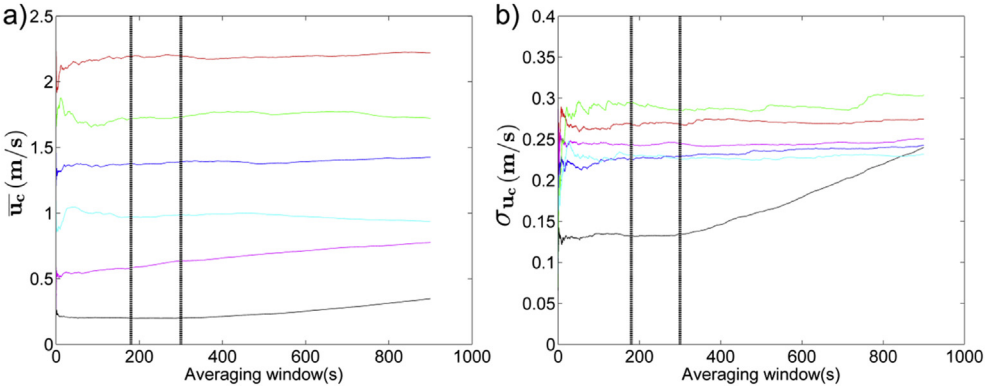

Fig. 2. Variation of (a) mean horizontal current speeds and (b) RMS of horizontal current speeds with current speed averaging window (WAT). The six different datasets were collected on 13 July 2011.

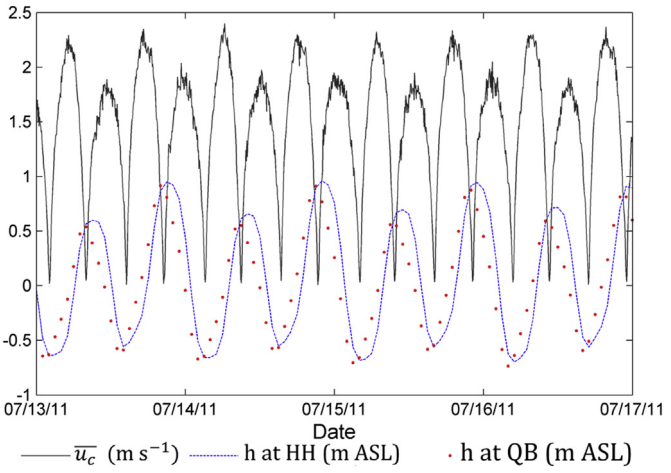

Fig. 3. Four-day time series of 5-minute averaged horizontal current speed and water surface levels for the two NOAA stations, the Horns Hook (HH) and Queensboro Bridge (QB) in New York, proximate to the RITE study site.

High regularity is desired by electric utilities because it allows accurate supply forecasting and scheduling. Tidal hydrodynamics are expected to be less regular at sites with more complex bed geometry like Admiralty Inlet in the Puget Sound, WA, USA, where close proximity to the headlands causes flow separation and shedding of vertically oriented vortices (eddies), resulting in multiple anharmonic currents that disrupt the otherwise sinusoidal shape in the tidal flow [7].

The peak horizontal current speeds ($\overline{u_{c_{max}}}$) for the entire POR at the Horns Hook station are shown in Fig. 4. The high water (HW), which includes both the higher high water (HHW) and lower high water (LHW), and the low water (LW), which includes both the higher low water (HLW) and lower low water (LLW), are also shown in the same figure. On average, the difference between the MHW and MLW is 1.39 m at the Horns Hook station and 1.28 m at the Queensboro Bridge station [30]. All peak flood and peak ebb current speeds are greater than 1.5 m s^{-1}, well above the 1.0 m s^{-1} turbine cut-in speed. The spring tidal current speeds, which occur around the full and new moon, are typically 0.5 m s^{-1} higher than the neap tidal current speeds, which occur around the first and third quarter moon. The peak ebb current speeds are consistently 15% less than the peak flood current speeds, which skews the power production towards the flood stage of the tide.

4.2. Current directions

The joint probability distribution (JPD) of the instantaneous horizontal current speeds (u_c) and the instantaneous current directions (θ) for the 20 Hz measurements is shown in Fig. 5a. The u_c values and θ values are discretized into 0.1 m s^{-1} and 1° bins. The solid white lines are the mean ebb direction ($\overline{\theta_{ebb}} = 15.1°$) and mean flood direction ($\overline{\theta_{flood}} = 195.9°$). The mean ebb direction ($\overline{\theta_{ebb}}$) was calculated iteratively with an initial value chosen arbitrarily. Subsequent mean ebb directions were obtained by averaging instantaneous current directions, with u_c values greater than 1 m s^{-1}, lying between $\overline{\theta_{ebb}} - 90°$ and $\overline{\theta_{ebb}} + 90°$. Iterations were continued until the mean ebb direction value converged. The mean flood direction for current speeds with $u_c > 1$ m s^{-1} was calculated using the same approach, but with a different data range, $\theta \in [\overline{\theta_{flood}} - 90° \cdot \overline{\theta_{flood}} + 90°]$. The mean ebb and mean flood current directions are nearly aligned with a phase difference of 180.8° (Fig. 5a).

The JPD plot in Fig. 5a shows several clusters with different current speeds, which indicates that the current directions are similar for a given value of current speed, but changes for different values of current speed. For the ebb tide, for example, the current directions are concentrated around 18° for u_c = 1.5 m s^{-1} and around 16° for u_c = 1.9 m s^{-1}. This variation is also observed in JPD plots constructed using a shorter POR. JPDs were constructed from five-minute averaged data measured during a rising limb (Fig. 5b), a peak tide (Fig. 5c), and a falling limb (Fig. 5d) in a single ebb cycle. The locations and intensities of the clusters are nearly identical for the rising limb plot (Fig. 5b) and the falling limb plot (Fig. 5d). In all four plots (Fig. 5a–d), clusters, which have the same current speeds, are in the same region of the JPD. The same pattern is observed for data measured during flood tides (not shown). These patterns indicate that the stage within the tidal cycle (rising, peaking, falling) has no influence on the variation of the current speed with the current direction. The variation of the current speed with the current direction, which is also shown on the JPD plots with a shorter POR, suggests that this variation is likely caused by turbulence. An abrupt change in current direction may change the rotor's orientation, which could adversely affect power generation and unsteady loading. The forces generated from small-scale turbulence, however, are generally too small to be able to change the rotor's orientation. Nonetheless, more research is needed to identify the turbulence time scales that are able to change the rotor's orientation.

The shape of the 5-minute current direction histogram (Fig. 5e) also changes with the mean current speed. In general, a higher current speed will lower the root-mean-square error of the current direction; as shown by the lower kurtosis value (higher peak and narrower width) for the peak tide histogram compared to the rising and falling limb histograms.

The average difference in current direction can be quantified using the root-mean-square (RMS) of the current directions (σ_θ). The RMS values for each of the current directions for ebb and flood flows were calculated using the same data domain used for $\overline{\theta_{ebb}}$ and $\overline{\theta_{flood}}$ calculations. The values of σ_θ are 8.6° for the flood tide and 10.1° for the ebb current. For fixed yaw turbines, changes in the current direction would result in reduction of the hydrokinetic power that can be extracted. Assuming a constant current speed of 2.5 m s^{-1}, a deviation in the current direction of 10° from the principal current alignment can decrease the generated power by 4.5%, while a deviation of 20° can decrease the generated power by 17%. This off-axis power was calculated using Eq. (2), with the projected off-axis velocity as an input [37].

Table 1
Major tidal current constituents and their amplitudes for the entire period of record (POR) calculated using the T_Tide Harmonic Analysis Toolbox [37].

Tidal current constituents	Period (solar hours)	Amplitude (m s^{-1})	Normalized amplitude
M2	12.421	1.569	1.000
N2	12.658	0.482	0.307
S2	12.000	0.127	0.081
K1	23.934	0.037	0.024
O1	25.819	0.031	0.020
M4	6.210	0.049	0.031
M6	4.140	0.015	0.009
S4	6.000	0.004	0.002
MS4	6.103	0.010	0.007

4.3. Horizontal current RMS and turbulence intensities

Turbulence intensity is a standard parameter in wind site classification for specifying the appropriate wind turbine design class and for predicting unsteady loads [38]. At the RITE site the

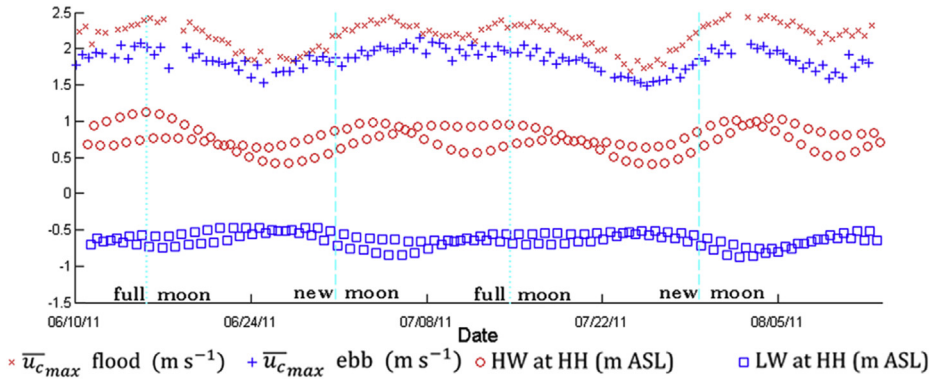

Fig. 4. Peak horizontal current speeds, high water (HW), and low water (LW) at Horns Hook tidal station for the study period.

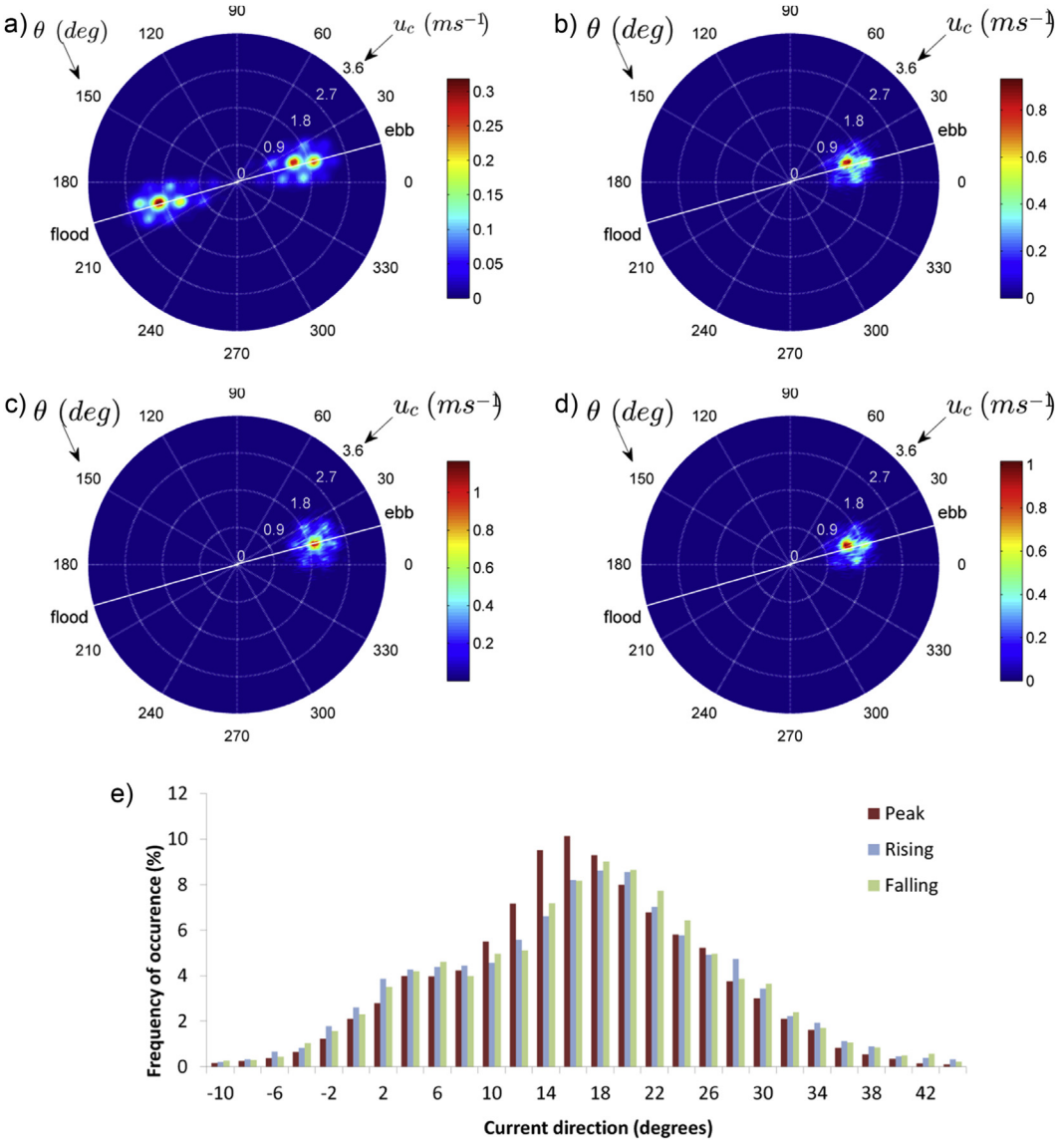

Fig. 5. Joint probability distribution (JPD) of instantaneous horizontal current speed (u_c) and direction (θ) at the study site for: (a) the entire POR, (b) a 5-minute period during a raising limb of an ebb tide ($\overline{u_c}$ = 1.48 m s^{-1}), (c) a 5-minute period during a peak ebb tide ($\overline{u_c}$ = 1.92 m s^{-1}), (d) a 5-minute period during a falling limb of an ebb tide ($\overline{u_c}$ = 1.50 m s^{-1}), and (e) the frequency histogram of the current directions for the rising, peak and falling ebb cases. The velocity bins for the JPD plots are in 0.1 m s^{-1} intervals and the direction bins are in 1° intervals. The solid white lines represent the principal directions of the mean flood and mean ebb current speeds ($\overline{u_c}$). The color code represents the fraction of samples in the bin out of the total number of samples. (For interpretation of the references to color in this figure legend, the reader is referred to the web version of this article.)

turbulence intensity ($I_{\overline{u_c}} = \sigma_{u_c}/\overline{u_c}$) is 15% at a reference mean current of 2 m s^{-1}, as shown in Fig. 6a. However, the $I_{\overline{u_c}}$ versus $\overline{u_c}$ relationship bifurcates for horizontal current speeds greater than 1.2 m s^{-1}, with higher turbulence levels for the same mean current speed occurring on the ebb tide. The higher turbulence levels observed on the ebb tide (Fig. 6a and b) are caused by the irregular channel geometry upstream of the ADV locations (Fig. 1a).

The turbulence intensity ($I_{\overline{u_c}}$) is a measure of the average turbulent fluctuations, normalized by the mean current speed ($\overline{u_c}$). Turbulence intensity values are typically inversely correlated with the mean current speed. For the study site, for example, $I_{\overline{u_c}}$ decreases from 23% at 1 m s^{-1} to 13% at 2.4 m s^{-1} on the flood tide as shown in Fig. 6a. The root-mean-square current speed (σ_{u_c}) is an absolute measure of the average turbulent fluctuations (not normalized), and is positively correlated with the unsteady loads. As shown in Fig. 6b, the decrease in the turbulence intensity ($I_{\overline{u_c}}$), in the previous example, coincides with an increase in the root-mean-square current (σ_{u_c}) from 0.24 m s^{-1} to 0.28 m s^{-1} during the peak flood; and 0.24 m s^{-1} to 0.33 m s^{-1} during the peak ebb. The root-mean-square current (σ_{u_c}), and therefore the unsteady loads, actually increase even though at, the same time, the turbulence intensity decreases.

The force density (*FD*) derived from the maximum instantaneous horizontal current speed (u_c), 6.3 kN m^{-2}, is twice of that derived from the maximum five-minute time-averaged current speed. The reason for this is the maximum instantaneous horizontal current speed, 3.5 m s^{-1}, is significantly higher than the maximum five-minute time-averaged current speed, 2.5 m s^{-1}. This observation highlights the importance of considering high frequency current speed measurements for determining extreme loads on TECs.

4.4. Turbulent kinetic energy

The spectral energy density (SED) plots for the instantaneous horizontal current speed (u_c) and instantaneous vertical current speed (w) are shown in Fig. 7. These plots were constructed from 474 individual five-minute time series measured on 13–15 July 2011 when u_c was greater than 1 m s^{-1}. The spectra were calculated using the Welch method in MATLAB [39]. Each 5-minute time series was divided into four segments using a window function (Hamming) [39], with a 50% overlap, and ensemble-averaged for eight degrees of freedom with a frequency bandwidth df = 0.0098 Hz. Three distinct regions are observed in Fig. 7: A low-frequency region (f < 0.1 Hz), where the turbulent kinetic energy

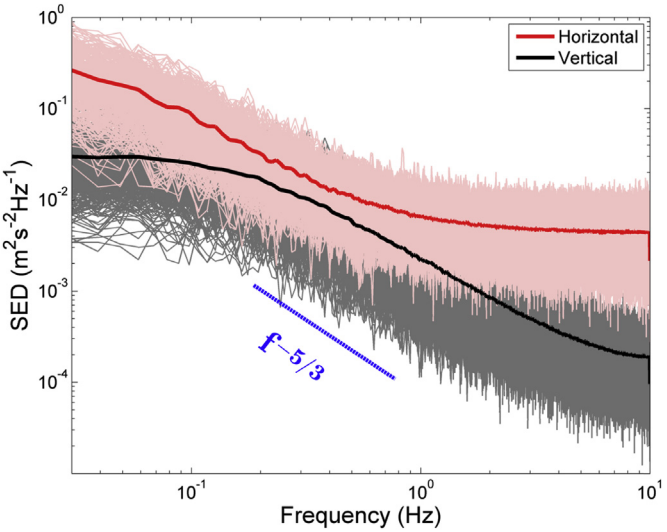

Fig. 7. Horizontal and vertical velocity spectral energy densities of 474 individual 5-minute velocity time series measured between 13 July 2011 and 15 July 2011 for u_c greater than 1 m s^{-1}. There were 4 ebb and 4 flood events during this measurement period. The spectra were calculated using the Welch method in MATLAB [39]. Each 5-minute time series was divided into four segments using a window function (Hamming) [39], with a 50% overlap, and ensemble-averaged for eight degrees of freedom with a frequency bandwidth df = 0.0098 Hz.

(TKE) content is highest, and horizontal components dominate over vertical components, indicating anisotropic turbulence; a mid-frequency region (0.2 < f < 0.5 Hz), which is the inertial sub-range where energy cascades, SED$\propto f^{-5/3}$, and horizontal and vertical components are nearly balanced; and a high frequency region contaminated by Doppler (instrument) noise, which resembles white noise. One would expect to have similar magnitudes of the SED components in the inertial sub-range, which is an indication of isotropic turbulence. This study shows differences in magnitudes between the horizontal and vertical component of the SEDs along the inertial sub-range. The smallest difference (less than 10^{-2} m^2 s^{-2} Hz^{-1}) is located between $2 \times 10^{-1} < f < 5 \times 10^{-1}$. The spectra flattening for the vertical component (S_{ww}) starts at a higher frequency (f = 2 Hz) than that for the horizontal component ($S_{u_cu_c}$) due to the relative orientation of the ADV acoustic beam angles for the vertical velocity component relative to the horizontal velocity component.

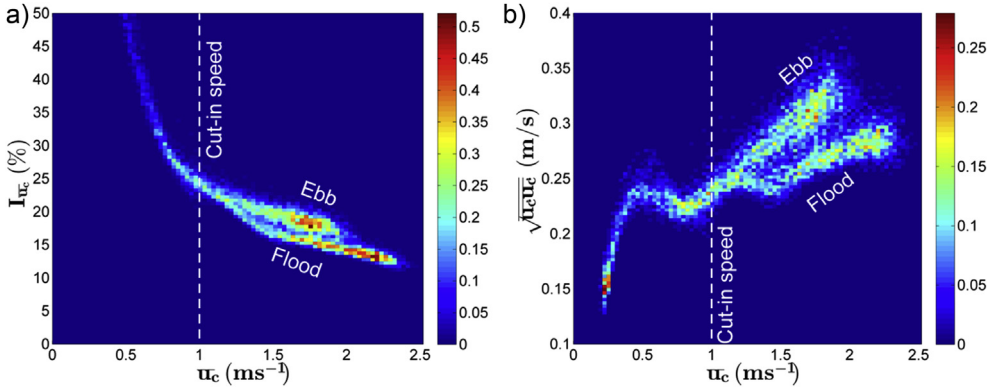

Fig. 6. Joint probability distribution of (a) turbulence intensity of the horizontal current ($I_{\overline{u_c}}$), calculated from one month of measurements at 20 Hz data output rate at the RITE study site, and (b) root-mean-square (RMS) of the horizontal current speed ($\sigma_{u_c} = \sqrt{\overline{u_c'u_c'}}$). The color indicates the fraction of the data out of the total number of samples, in percent. (For interpretation of the references to color in this figure legend, the reader is referred to the web version of this article.)

4.5. Effect of temporal averaging of current speed on force and power densities

The values of *FD* and *PD* calculated using Equations (1) and (2) are highly influenced by the window averaging time (WAT) used to calculate the mean current speed (input variable for the equations). To investigate the sensitivity of *FD* values on the WAT, normalized mean and maximum *FD* values were plotted against WATs that range from 1/20 s (not averaged) to 1 day. All mean *FD* values were normalized using the mean *FD* value calculated using the reference mean current speed. All maximum *FD* values were normalized using the maximum *FD* value calculated using the reference maximum current speed. The same approach is also used for plotting the normalized mean and maximum *PD* values. The reference mean current speed and reference maximum current speed are derived using a one second WAT. This particular WAT value was selected based on Chamorro et al. [40]. Chamorro et al. [40] suggests that the fluctuations in the turbine power time-series are sensitive to the inflow turbulence features at the low frequency bands bounded by a critical frequency f_c, approximately 1.5 times the turbine rotational frequency (f_T). With a typical rotational frequency of 0.67 Hz, the Gen5 turbine has a critical frequency of 1 Hz. The inverse of the critical frequency, one second, was selected as the reference WAT value.

In order to determine the relationship between the turbulence length scales at the site and the critical frequency, the turbulence integral time scales for 3700 five-minute time series were calculated using the autocorrelation function of the current speed time series. The average integral time scale was 0.2 s ($f = 5$ Hz), smaller than the inverse of critical frequency (f_c), where $1/f_c = 1$ s. Applying Taylor's frozen hypothesis, the integral length scale is ≈ 0.4 m, well below the flow depth (upper bound of the length scale), and is equivalent to approximately 8% of the turbine rotor diameter. In other words, the transition from large scale eddies to isotropic eddies takes place at scales significantly less than the rotor diameter.

It can be shown that the mean and maximum *FD* and *PD* values are under-predicted when using the mean current speed ($\overline{u_c}$) in place of the instantaneous current speed u_c [2]. This under-prediction is illustrated in Fig. 8a–d. Using the instantaneous current speed (u_c), the mean *FD* is 3% greater than the reference mean *FD* and the mean *PD* is 7% greater than the reference mean *PD* (Fig. 8a–b). The maximum *FD* and maximum *PD* values are 35% and 57% higher than their reference values when calculated using the instantaneous horizontal current speed (Fig. 8c and d). In general, Fig. 8a–d shows an inverse correlation between the WAT and all of these variables: the mean *FD*, the mean *PD*, the maximum *FD* and the maximum *PD*. These observation show that the choice of the averaging window (or temporal resolution) of the current speed can significantly affect the mean and maximum values of force and power density and, therefore, should be carefully chosen when designing TECs.

4.6. Force and power densities at the study site

The frequency distribution of the instantaneous horizontal current was examined by constructing the frequency and cumulative frequency histograms shown in Fig. 9. The cumulative frequency histogram shows that the instantaneous horizontal current was greater than the turbine cut-in speed for 75% of the time, indicating the turbine would be operational most of the time. This histogram also shows that the turbine design (rated) speed, 2.1 m s^{-1}, lies in the 16% exceedance level (i.e. only 16% of current speeds are equal to or greater than the rated speed). The mean

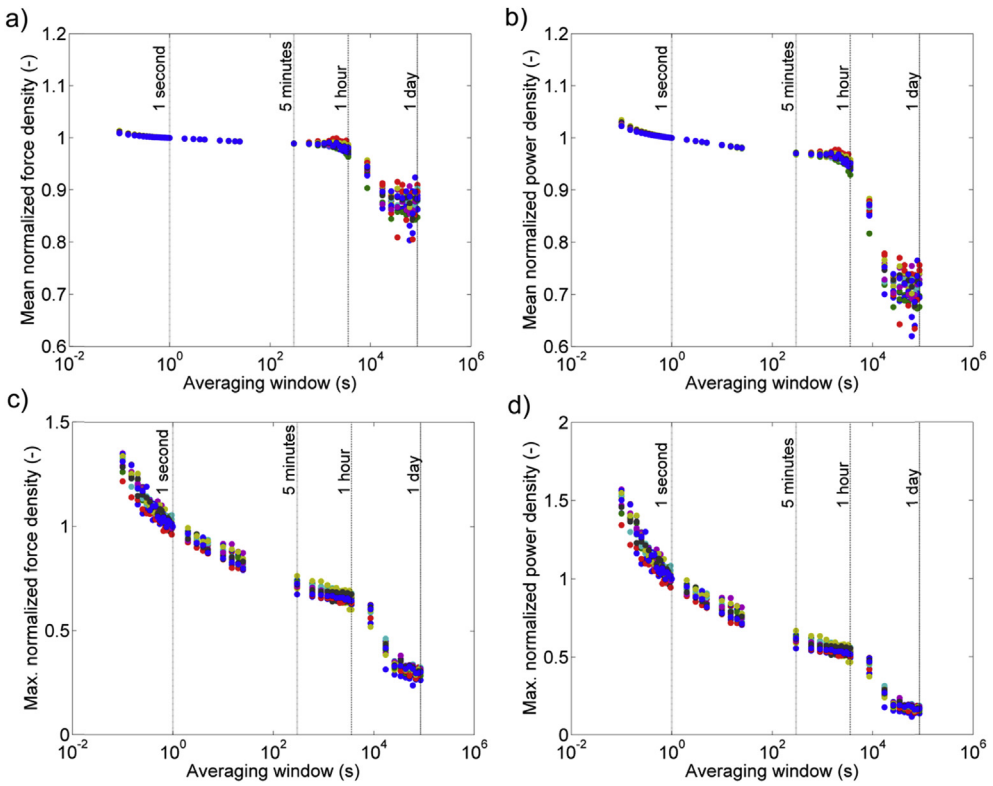

Fig. 8. Mean and maximum normalized force and power densities with respect to horizontal current averaging windows calculated from 15 different time series (shown in different colors). Force and power density values were normalized with their respective 1 s values (for each time series). The lengths of the time series range from 0.68 to 3.37 days, with a mean and a median value of 2.15 and 2.07 days, respectively. (For interpretation of the references to color in this figure legend, the reader is referred to the web version of this article.)

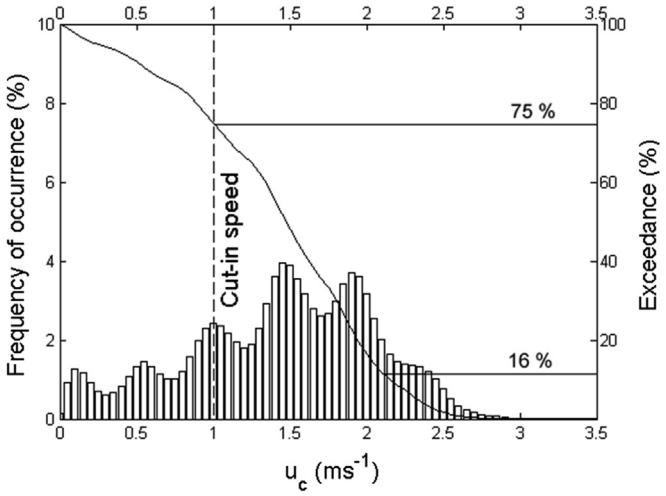

Fig. 9. Frequency histogram (bar) and cumulative frequency histogram (line) of horizontal current at the RITE site.

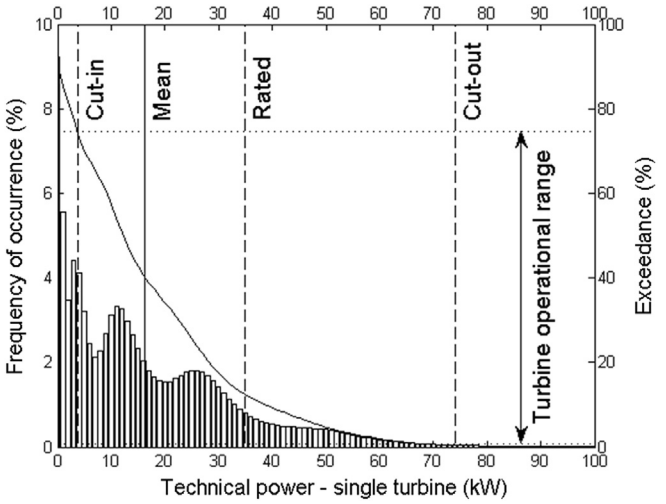

Fig. 10. Frequency histogram (bar) and cumulative frequency histogram (line) of electrical power for a single Verdant Gen5 turbine.

theoretical *PD* values over the one month period (when the ADV sampling rate was set to 20 Hz) were calculated from the instantaneous and one second-averaged horizontal current speeds. The results do not differ significantly: 2.31 kW m^{-2} for the 1/20 s WAT (instantaneous) and 2.26 kW m^{-2} for the one second WAT (averaged). These values, however, are an order of magnitude higher than the mean *PD* values reported in the national tidal energy resource assessment map [3,5], which range between 0.1 and 0.4 kW m^{-2}. This large discrepancy is due to the coarse spatial and temporal resolution of the model used to estimate the tidal energy resource assessment, which causes low pass filtering, which in turn, reduces power density estimates.

A turbine can only extract a portion of the *theoretical power* of the tidal current resource available due to technical limitations, which include turbine efficiency, drivetrain efficiency, generator efficiency, power conditioning efficiency [41], cut-in speed and cut-out speed. For a single turbine, the power density needs to be multiplied by the EEP of the turbine. The rated power for the Gen5 turbine is 35 kW, but the turbine was designed to generate electricity up to 74 kW. The calculated mean electrical power of a single Verdant Gen5 turbine at the study site, with a rotor radius of 2.5 m, is 16.3 kW. This was calculated after assuming a water to wire efficiency of 0.38, a cut in power of 3.8 kW and a cut-off power of 74 kW (Fig. 10).

5. Conclusions

The present study contributes to a growing catalog of tidal energy site resource assessments by examining the temporal variability, frequency, direction and magnitude of the mean current, turbulence, hydrodynamic force, and tidal power for an emerging MHK industry. The temporal variations, mean current statistics, turbulence and power density are examined in detail, and reveal the regular semi-diurnal characteristics of mean horizontal current speeds at the RITE site. The power production is skewed towards the flood tide, due to the consistently higher flood current speed, relative to that of the ebb current.

It has been shown that the values of theoretical force and power densities are significantly influenced by the WAT selected for calculating the input mean current. Using a shorter WAT will generally increase the force and power densities. For estimating the mean theoretical force and power densities from site measurements, the WAT should ideally be equivalent to the smallest turbulence time scale that contributes to the fluctuation of the turbine power generation time series. The relevant turbulence time scales for describing unsteady loads may be smaller and therefore, may require a shorter WAT. Furthermore, since the maximum force is generally found when the shortest WAT is used, it may be prudent to calculate the maximum load for device design using the instantaneous (ADV) current measurements until the range of turbulence scales that affect power generation and loading is better understood.

Comparisons between ADV measurements at the RITE site and the national tidal resource assessment show a significant underestimation of theoretical power density by the latter, due to the coarse spatial and temporal resolution of the model used to estimate the tidal energy resource assessment. We therefore recommend that, while national (large-scale) resource assessments are useful, measurements at the device scale are needed to accurately estimate the hydrodynamic loads and power density at proposed tidal energy sites.

The regularity and predictability of the tidal current is a desirable feature at hydrokinetic energy sites that allows accurate forecasting of the electricity supply. A summary statistic that quantifies the degree of regularity for tidal energy site classification, such as the root-mean-square difference between the tidal velocity time series and a sinusoidal function, is therefore recommended.

As with the wind industry, which has an International Electrotechnical Commission (IEC) wind class standard to aid in the selection of wind turbines for a particular site, it is recommended that the tidal energy industry move forward to develop an appropriate standard for tidal current classes. Such a standard would quantify key site parameters, as demonstrated here, to enable a direct comparison between potential project locations, ultimately improving device performance and survivability in a variety of operating conditions. Development of this standard requires selection of a list of tidal energy sites that exhibit the range of hydrodynamic conditions that will be encountered, a comprehensive field campaign at multiple tidal energy sites that can identify the key hydrodynamic parameters for tidal current site classification and adoption of consistent measurement practices.

Acknowledgments

This research was supported by the U.S. Department of Energy's (DOE) Office of Energy Efficiency and Renewable Energy, Wind and

Water Power Technologies Program under the DOE Advanced Water Power Project Grant No. DE-FG36-08GO18168/M001, the DOE Advanced Water Power Project Contract No. DE -FG36-08GO18168.005, titled: *"Improved Structure and Fabrication of Large, High-Power KHPS Rotors."* Sandia National Laboratories is a multi-program laboratory managed and operated by Sandia Corporation, a wholly owned subsidiary of Lockheed Martin Corporation, for the U.S. Department of Energy's National Nuclear Security Administration under contract DE-AC04-94AL85000. The authors thank Dean Corren and Mary Ann Adonizio of Verdant Power, as well as the reviewers of this paper, for their helpful comments and suggestions.

Notation

A	energy extraction plane, m^2
A_c	channel cross section area, m^2
d_T	turbine rotor diameter, m
f	frequency of the spectral energy density, Hz
f_c	turbine critical frequency, Hz
FD	hydrodynamic force density, N m^{-2}
f_T	turbine rotational frequency, Hz
h	mean water level above sea level, m
$I_{\overline{u_c}}$	turbulence intensity of the horizontal current speed, (dimensionless)
P_c	channel wetted perimeter, m
PD	power density, W m^{-2}
ρ	fluid density, kg m^{-3}
r	rotor radius, m
R	A_c/P_c, hydraulic radius, m
Re	$4\,\overline{u_c}\,R/\upsilon$, Reynolds number, (dimensionless)
$S_{u_cu_c}$, S_{ww}	velocity spectral energy densities of horizontal and vertical current speeds, $m^2\ s^{-2}\ Hz^{-1}$
T	wave period of one sinusoidal cycle, second or hour
θ, $\overline{\theta}$	instantaneous and time-averaged horizontal current direction, degrees
u, v, w	instantaneous longitudinal, lateral, and vertical velocities, m s^{-1}
u_c, $\overline{u_c}$	instantaneous and time-averaged horizontal current speed, m s^{-1}
$\overline{u_{c_{max}}}$	time-averaged maximum horizontal current speed, m s^{-1}
σ_{u_c}	time-averaged root-mean-square (RMS) of horizontal current speeds, m s^{-1}
σ_θ	root-mean-square (RMS) of the current directions, degrees
υ	kinematic viscosity, $m^2\ s^{-1}$ ($1.05 \times 10^{-6}\ m^2\ s^{-1}$ for sea water at 20C)
x, y, z	longitudinal, lateral, and vertical coordinate distance, m
z_{hub}	distance from the turbine hub height to channel bed, m

References

[1] Gooch S, Thomson J, Polagye B, Meggitt D. Site characterization for tidal power. In: OCEANS 2009, MTS/IEEE Biloxi – Marine Technology for Our Future: Global and Local Challenges; 2009. pp. 1–10.
[2] Neary VS, Gunawan B, Sale DC. Turbulent inflow characteristics for hydrokinetic energy conversion in rivers. Renew Sustain Energy Rev 2013;26:437–45.
[3] Defne Z, Haas KA, Fritz HM, Jiang LD, French SP, Shi X, et al. National geodatabase of tidal stream power resource in USA. Renew Sustain Energy Rev 2012;16:3326–38.
[4] Georgia Tech Research Corporation. Assessment of energy production potential from tidal streams in the United States. Final Project Report; 2011.
[5] Georgia Tech Research Corporation. Assessment of energy production potential from tidal streams in the United States. Georgia Institute of Technology; 2011 [accessed 20.12.12], http://www.tidalstreampower.gatech.edu/.
[6] Neary VS, Gunawan B, Polagye B, Thomson J, Richmond MC, Durgesh V, et al. Field measurements at river and tidal current sites for hydrokinetic energy development: best practices manual. ORNL/TML-2011/419, 2011.
[7] Thomson J, Polagye B, Durgesh V, Richmond MC. Measurements of turbulence at two tidal energy sites in Puget Sound, WA. IEEE J Ocean Eng 2012;37:363–74.
[8] Polagye B, Thomson J. Tidal energy resource characterization: methodology and field study in Admirality Inlet, Puget Sound, US. Proc Inst Mech Eng Part A J Power Energy May 2013;227(3):352–67.
[9] Richmond MC, Durgesh V, Thomson J, Polagye B. Inflow characterization for marine and hydrokinetic energy devices. FY-2011: Annual Progress Report PNNL-20463, 2011.
[10] Easton MC, Harendza A, Woolf DK, Jackson AC. Characterisation of a tidal energy site: hydrodynamics and seabed structure. In: 9th European Wave and Tidal Energy Conference, Southampton, UK; 2011.
[11] Milne IA, SHarma RN, Flay RGJ, Bickerton S. Characteristics of the turbulence in the flow at a tidal stream power site. Phil Trans R Soc A 2013;371. no. 1985 20120196.
[12] Goddijn-Murphy L, Woolf DK, Easton MC. Current patterns in the inner sound (Pentland Firth) from underway ADCP data. J Atmospheric Ocean Technol 2012;30:96–111.
[13] Bahaj AS. Generating electricity from the oceans. Renew Sustain Energy Rev 2011;15:3399–416.
[14] Jonkman BJ. TurbSim user's guide, version 1.50. Technical Report NREL/TP-500–46198. National Renewable Energy Laboratory, 2009.
[15] Jonkman JM, Buhl ML. FAST user's guide. National Renewable Energy Laboratory. Technical Report NREL/EL-500–38230. National Renewable Energy Laboratory; 2005.
[16] Murray JC, Barone M. The development of CACTUS, a wind and marine turbine performance simulation code. In: The 49th Aerospace Sciences Meeting. Orlando, Florida: American Institute of Aeronautics and Astronautics; 2011.
[17] Neary VS, Gunawan B, Hill C, Chamorro LP. Near and far field flow disturbances induced by model hydrokinetic turbine: ADV and ADP comparison. Renew Energy 2013;60:1–6.
[18] Gunawan B, Sterling M, Knight DW. Using an acoustic Doppler current profiler in a small river. Water Environ J 2010;24:147–58.
[19] Muste M, Yu K, Spasojevic M. Practical aspects of ADCP data use for quantification of mean river flow characteristics; part I: moving-vessel measurements. Flow Meas Instrum 2004;15:1–16.
[20] Stone MC, Hotchkiss RH. Evaluating velocity measurement techniques in shallow streams. J Hydraulic Res 2007;45:752–62.
[21] Szupiany RN, Amsler ML, Best JL, Parsons DR. Comparison of fixed- and moving-vessel flow measurements with an aDp in a large river. ASCE J Hydraulic Eng 2007;133:1299–309.
[22] Palodichuk M, Polagye B, Thomson J. Resource mapping at tidal energy sites. J Ocean Eng 2013;38:433–46.
[23] Stacey MT, Monismith SG, Burau JR. Measurements of Reynolds stress profiles in unstratified tidal flow. J Geophys Res Oceans 1999;104:10933–49.
[24] Colby JA, Corren D. Detailed inflow measurements for kinetic hydropower systems in a tidal strait. In: Hydrovision; 2010.
[25] Colby JA, Adonizio MA. Hydrodynamic analysis of kinetic hydropower arrays. In: Waterpower XVI; 2009. no. 204.
[26] Li Y, Colby JA, Kelley N, Thresher R, Jonkman B, Hughes S. Inflow measurement in a tidal strait for deploying tidal current turbines: lessons, opportunities and challenges. In: ASME Conference Proceedings, 2010; 2010. pp. 569–76.
[27] Power Verdant. Roosevelt Island tidal energy project. FERC No. P-12611 – Final kinetic hydropower pilot license application, 2010.
[28] Pugh DT. Tides, surges, and mean sea-level. J. Wiley; 1987.
[29] Spurlock DS. Modeling flows for assessing tidal energy generation potential. Civil Engineering, Virginia Polytechnic; 2008.
[30] National Oceanic and Atmospheric Administration. Tidal and current data http://tidesandcurrents.noaa.gov; 2012.
[31] Nezu I, Nakagawa H. Turbulence in open channel flows. Taylor & Francis; 1993.
[32] Garcia CM, Cantero MI, Nino Y, Garcia MH. Turbulence measurements with acoustic Doppler velocimeters. ASCE J Hydraulic Eng 2005;131:1062–73.
[33] Goring DG, Nikora VI. Despiking acoustic Doppler velocimeter data. J Hydraulic Engineering-Asce 2002;128:117–26.
[34] Gunawan B, Neary VS, McNutt JR. ORNL ADV post processing guide and Matlab algorithms for MHK site flow and turbulence analysis. ORNL/TML-2011/338, 2011.
[35] Bowman MJ. The tides of the East River, New York. J Geophys Res 1976;81:1609–16.
[36] Pawlowicz R, Beardsley B, Lentz S. Classical tidal harmonic analysis including error estimates in MATLAB using T_TIDE. Comput. Geosci 2002;28:929–37.
[37] Pedersen TF. On wind turbine power performance measurements at inclined airflow. Wind Energy 2004;7:163–76.
[38] International Electrotechnical Commission. Wind turbines – part 1: design requirements. IEC 61400–1 ed 3.0, 2005.
[39] MATLAB, version 7.14.0.739 (R2012a). The MathWorks Inc.; 2012.
[40] Chamorro LP, Hill C, Morton S, Ellis C, Arndt REA, Sotiropoulos F. On the interaction between a turbulent open channel flow and an axial-flow turbine. J Fluid Mech 2012. http://dx.doi.org/10.1017/jfm.2012.571.
[41] Hagerman G, Polagye B, Bedard R, Previsic M. Methodology for estimating tidal current energy resources and power production by tidal in stream energy conversion (TISEC) devices. EPRI-report, 2006.